Integrated placental modelling of histology with gene expression to identify functional impact on fetal growth

Hannah Ee Juen Yong[1,2]*, Kasia Maksym[3,4]*, Muhammad Ashraf Bin Yusoff[3], Esteban Salazar-Petres[1], Tatiana Nazarenko[3,5], Alexey Zaikin[3,5], Anna L David[3,4,6], Sara L Hillman[3,4]+, Amanda Nancy Sferruzzi-Perri[1]+

*contributed equally; joint first author

+contributed equally; joint last and corresponding author

[1]Centre for Trophoblast Research,

Department of Physiology, Development and Neuroscience

University of Cambridge

Cambridge UK

CB2 3EG

[2]Singapore Institute for Clinical Sciences,

Agency for Science, Technology and Research,

Singapore

[3] Elizabeth Gareth Anderson Institute for Women's Health,

University College London,

84-86 Chenies Mews, London UK

WC1E 6HU

[4] Fetal Medicine Unit

Elizabeth Gareth Anderson Wing,

University College Hospitals NHS Trust,

25 Grafton Way, London UK

WC1E 6DB

[5] Department of Mathematics,

University College London,

London UK

WC1E 6AE

[6] National Institute for Health Research University College London Hospitals Biomedical Research Centre, 149 Tottenham Court Road, London W1T 7DN

Correspondence:

Amanda Sferruzzi-Perri

[1]Centre for Trophoblast Research,

Department of Physiology, Development and Neuroscience

University of Cambridge

Cambridge UK

CB2 3EG

+44 (0) 1223 333 807

ans48@cam.ac.uk

Sara Hillman

Elizabeth Gareth Anderson Institute for Women's Health,

University College London,

84-86 Chenies Mews, London UK

WC1E 6HU

+ 44 (0)203 447 6162

sara.hillman@ucl.ac.uk

Conflicts of interest

The authors have declared that no conflict of interest exists

Abstract:

Fetal growth restriction (FGR) is a leading cause of perinatal morbidity and mortality. Altered placental formation and functional capacity are major contributors to FGR pathogenesis. Relating placental structure to function across the placenta in healthy and FGR pregnancies remains largely unexplored but could improve understanding of placental diseases. We investigated integration of these parameters spatially in the term human placenta using predictive modelling. Systematic sampling was able to overcome heterogeneity in placental morphological and molecular features. Defects in villous development, elevated fibrosis, and reduced expression of growth and functional marker genes (insulin-like growth factor-2, vascular endothelial growth factor-A, solute carrier family 38 member 1, solute carrier family 2 member 3) were seen in age-matched term FGR versus healthy control placentas. Characteristic histopathological changes with specific accompanying molecular signatures could be integrated through computational modelling to predict if the placenta came from a healthy or FGR pregnancy. Our findings yield new insights into the spatial relationship between placental structure and function and the aetiology of FGR.

Key words: Placenta, FGR, modelling, morphology, growth genes, transport

Introduction:

The human placenta is a highly specialized organ in pregnancy, whereby normal functioning is critical to fetal development and long term health. By acting as a functional interface between the maternal and fetal circulation, it is responsible for maternal-fetal substrate exchange, protects the fetus from immune rejection by the mother and secretes hormones, which maintain pregnancy and promote healthy fetal growth and development (1, 2). This complex organ is structurally heterogeneous, not only in terms of its broad spatial macroscopic characteristics with multiple cotyledons and vascular supply, but also at the microscopic level of the villous tree and trophoblast. Even in pregnancies that deliver at term without any apparent pathology, novel techniques such as micro-CT are now describing the large degree of heterogeneity of vascular density and branching in the placenta (3). In addition, computational models have predicted that local heterogeneity in placental vascular structure can have major impacts on the resistance of the feto-placental circulation and placental dysfunction (4). Investigating the spatial relationships between changes in gene expression and structural differences in the placenta is important, so that we may better elucidate the potential functional effect of placental pathology in obstetric disease.

Fetal growth restriction (FGR) is a major cause of perinatal morbidity and mortality. The risk of *in utero* or neonatal death is especially high amongst growth restricted fetuses and neonates who are commonly born preterm (https://www.who.int/publications/i/item/every-newborn-an-action-plan-to-end-preventable-deaths). In some regions of the world, FGR and prematurity accounts for 80% of neonatal deaths (5). FGR is diagnosed when a fetus fails to reach their genetically predefined growth potential and is often identified by feto-placental ultrasound features (such as increased umbilical artery resistance to blood flow), and subsequently

confirmed through placental histopathology (6). The gestational age at diagnosis is used to further subdivide FGR into early-onset, detected before 32 weeks of gestation, and late-onset according to international consensus (7). Neonates born following FGR have an increased risk of developing health problems, both in the immediate postnatal period including low blood sugars and poor temperature regulation and feeding, but also in later adult life in the form of cardiovascular and metabolic disease (8, 9). Management of pregnancies affected by FGR can be challenging, as timing of delivery needs to be judged well, to balance the hazards of preterm birth against the risks of irreversible damage secondary to intrauterine hypoxia and nutritional deficiency or even stillbirth (10).

The placenta of FGR pregnancies is characterized by reduced syncytiotrophoblast surface area, increased thickness of the exchange barrier formed by the trophoblast and fetal capillary endothelium and an increase in placental apoptosis (11-14). This complex series of adaptations in response to dysfunctional placentation affects the ability of the placenta to provide sufficient oxygen and nutrients to the fetus, which in turn, is thought to compromise fetal growth and development. Whilst it is recognized that there are key mediators of fetal growth that are influenced by placental function including but not limited to transfer of gases (15), glucose (16, 17), lipids (18) and amino acids (17, 19), direct cause and effect is not clear. Nuanced, integrated investigations are required to better delineate the underlying functional mechanisms related to the histological changes observed in the placenta. Experimental animal data has highlighted central roles that certain structural and functional changes play in the placenta to fetal growth outcomes (20-24). However, data on how structure *and* molecular changes together impact on function and on each other, even in the form of nutrient transporter expression, are scarce or not available for the human placenta (25, 26).

Better understanding of how placental structure relates to functional capacity is also furthered through optimized and robust placental sampling protocols. Methodological errors arise from differences in sampling and/or tissue processing, which has previously hampered the reproducibility and possible extrapolation of placental studies (27, 28). Systematic uniform random sampling involves random selection of the first sampling site, with subsequent sites dictated by a pre-made sampling interval. This method is recommended to ensure representative and unbiased sampling of the placenta (28, 29). It is a simple method, allowing for even coverage of the placenta and ensures that all sites can only be selected once (28). In practice, however, systematic uniform random sampling has limitations. Firstly, its lack of bias may be compromised if the pre-determined sampling interval coincides with a natural pattern existent in the placenta (29). Secondly, placentae templates designed for systematic uniform random sampling assume all placentas to be roughly circular in shape, with central umbilical cord insertion. This assumption of a uniform shape and cord insertion however is incorrect. Although studies do show that mean placental chorionic shape at term is round, deviations in placental shape are associated with reduced placental efficiency (30). In addition, the point of umbilical cord insertion appears to affect placental function, with a marginal cord insertion near the outer boundary of the placenta resulting in a more asymmetric chorionic vessel structure (31), which has been associated with FGR, stillbirth and neonatal death (32).

While analysis of single sites may miss important histopathological and functional changes, multiple site collection poses analytical challenges, and methods may still fail to identify critical differences within placentas affected by pathology, such as FGR. Statistical modelling allows for the exploration and integration of multiple data points from the same sample to provide more accurate interpretation of functional consequences. Moreover, the use of modelling to predict regional and disease state differences has high translational potential, for

example providing an explanation for why the pregnancy was compromised and which baby may benefit the most from early health monitoring and/or intervention. With this study we therefore, firstly sought to better understand if systematic uniform random sampling methods could be optimised to the challenges FGR placentas pose. Secondly, we sought to characterise the degree of detailed histological and molecular heterogeneity between multiple placental samples in healthy and FGR placentas. Finally, we examined potential links between histological changes and the expression of genes involved in placental formation, transport, and transcriptional regulation, and their relationships with fetal growth/pregnancy outcome by incorporating novel modelling analysis to better delineate the significance of the placenta in health and disease.

Results:

Patient characteristics

We matched FGR cases and controls for maternal age, booking BMI, mode of delivery and infant sex (Table 1) with expanded clinical data available (Supplementary Table 1). Nonetheless, several significant differences in clinical characteristics were still observed. FGR cases were more likely to be non-White and delivered infants with lower birth and placental weights about a week earlier, although all delivered at term ($>36^{+6}$ weeks of gestation).

Stereological analysis of placental morphology

Comparing stereological findings by sampling site within the FGR or control groups showed no significant differences between samples taken from the central and peripheral regions of the placenta (Supplementary Table 2). Hence, we averaged the data of the central and peripheral regions of each placenta to compare by pathology (Table 2). Taking into consideration a false discovery rate of 5% for multiple testing, FGR placentas had significantly lower volume

densities of intermediate villi, syncytial knots and higher volume densities fibrosis and capillaries. Once placental weight was accounted for, FGR cases showed decreased volumes of intervillous spaces, intermediate villi, terminal villi, syncytial knots, trophoblast and stromal components, and increased volume of fibrosis compared to control placentas. There were no differences in any measure of barrier thickness, surface area, surface densities and diffusion capacities between FGR and control placentas; except that FGR placentas had a decreased villi surface area.

Placental expression of growth factors and nutrient transporters

We also evaluated relative mRNA expression of selected growth factors and nutrient transporters (Figure 1) that have been previously implicated in transcriptional control or with compromised fetal growth in humans and animal models of FGR (33-38). Placental *IGF2*, *SLC2A3* and *SLC38A1* expression was significantly lower for FGR versus controls, regardless of sampling location (Figures 1A, 2D and 2E). *VEGFA* expression was significantly lower in the peripheral region as compared to the central region of FGR placentas, while no statistical difference was identified in the central region between cases and controls (Figure 1B). Only *SLC2A1* expression was significantly increased in FGR placenta as compared to controls, independent of sampling location (Figure 1C). No differences in mRNA expression of and *SLC38A2* were observed between FGR and control placentas or by sampling location (Figure 1F). In controls, placental *HNF1A* expression was higher in the peripheral region as compared to the central region (Figure 1G), but no differences were identified for FGR.

Associations between placental morphology and expression of functional genes

We next evaluated relationships between placental morphology and the expression of growth factor and nutrient transporter genes within the different sampling sites, and between control

and FGR groups using Pearson's r coefficient (Figure 2). In FGR placentas, several inverse correlations were identified between expression of *IGF2, VEGFA, SLC38A1* and *SLC2A3* and the volume of terminal villi, trophoblast, and capillary volume predominantly in the peripheral region of FGR placentas. Inverse correlations with fibrosis volume were also observed for expression *IGF2, VEGFA, SLC38A1* and *SLC2A3* in the central region of FGR placentas. Additionally, the relative expression of *IGF2, VEGFA, SLC38A1* and *SLC2A3* genes was inversely correlated with barrier thickness uniformity index and both maternal blood spaces and fetal capillaries surface densities in the FGR placenta (central and peripheral sites), although no significant correlations were detected for the control placenta. Moreover, the expression of *IGF2, SLC38A1* and *SLC2A3* genes negatively correlated with both theoretical and specific diffusion capacity in FGR, but not control placentas. In contrast, FGR expression of *HNF1A* showed a positive correlation with specific diffusion capacity in the peripheral region. Positive correlations between the expression of all genes measured and fibrosis and stromal volumes were found for the peripheral region of control placentas, but not FGR placentas. Positive relationships were also seen for expression of VEGFA and HNF1A with the stem villi volume in central sites of control placentas.

Predictive modelling

To evaluate the information gained from different placental regions/sampling sites (only peripheral, only central, or both together) and data types (only stereological data, only qPCR data or both together), we considered all their possible combinations using predictive modelling (construction of classifiers that would make it possible to distinguish patients in the control group from patients with FGR). As predictive modelling was carried out using three machine learning (ML) methods; *xgbTree*, *glmnet* and *nnet*, this resulted in 27 models for consideration. The binary outcome of FGR was used as an outcome with chosen set of features

(only stereological data, only qPCR data, both data types together) used as predictors. The predictive performance of each model was assessed using a leave-one-out cross-validation (LOOCV) scheme: the prediction was made for each patient (with all measurements) by excluding (withholding) it from the dataset, training the classifier on the remaining (independent) samples, and then generating predictions for the withheld samples using the trained model. Using predictions on the training subset (on each round of LOOCV procedures), the best threshold (corresponding to the best sum of sensitivity plus specificity) distinguishing controls from FGR cases was found and a binary result was calculated for each withheld sample (1 indicated FGR if the prediction was above the threshold, and 0 indicated control if it was below the threshold). Through all rounds, LOOCV procedure binary results were collected for withheld samples and performance was assessed using by these sets of predictions. Performance was estimated using areas under the ROC curve (AUCs) in 2 ways: "AUC for all samples" and "AUC for all patients", as described in Methods. For each combination of "placenta part + type of measurement + ML model" two such AUC values were obtained. Full results of these analyses can be found in Table 3 (in addition, we provide a complete table of errors for each patient in Supplementary Table 3). For a simplified visualization of these results, we considered the distributions of results (AUCs) of different types of ML models on different types of data obtained in different parts of the placenta for all patients and for all their samples separately (Figure 3). This plot clearly shows that among the considered models, the best are those based on measurements performed on the peripheral parts of the placenta and using stereological and qPCR data together. As shown in Table 3, the best model was found to be *nnet*, i.e., the model using simple artificial neural networks for a classification. This model gave the best result for both "AUC for all samples" (0.979) and "AUC for all patients" (0.917). By considering the stereological and qPCR data separately, the stereological data showed a greater predictive power than the qPCR data (Figure 3, for all variants), which, may be due to

the clearly different interdependences of the stereological parameters of the control group and the FGR group (the most significant interdependences are presented in Supplementary Figure 1). However, a combination of stereology and qPCR data works better than just stereology for analyses on peripheral parts of the placenta (Figure 3). The results obtained on the central parts of the placenta were lower than the results obtained on both parts of the placenta or only on the peripheral (boxplots for the central parts are slightly lower than the other options). Moreover, results using only peripheral parts were better than using a combination of both parts. Thus, the best model would be that based on measures made on the peripheral parts of the placenta using stereological and qPCR data together.

Discussion

There was no significant variability in the morphological features of the placenta within and between the peripheral and central sites of the placenta, regardless of whether they came from a healthy or FGR pregnancy. In addition, the findings indicate that alterations in placental morphology may be uniform across the placenta in late-onset FGR pregnancies without other complications, such as pre-eclampsia, that can lead to more variable histological changes across the placenta (39).

Despite established evidence that the placenta drives a number of the 'great obstetrical' syndromes, which includes FGR, the relatively poor understanding of underlying placental mechanisms makes interpretation of how they contribute to clinical presentations difficult (40). Heterogeneity within the placenta is thought to be responsible for some of the difficulties in directly relating disease state to placental findings. Our results suggest that the systematic sampling technique that we used, was able to overcome potential morphological spatial heterogeneity of the term placenta. Indeed, peripheral versus central region comparisons

277 revealed unique features in gene expression correlations and predictive modelling results.
278 These findings enable more clinical interpretations to be made of the results and that use of the
279 same sampling technique may allow for improved reproducibility between placental studies.
280
281 Morphological differences between the control and FGR placenta are consistent with findings
282 of others (41), and indicate villous maldevelopment, with fewer mature intermediate and
283 terminal villi and reduced villous surface area, as well as elevated fibrosis. The increased
284 villous capillary density and reduced syncytial knots in the studied FGR placentas are novel
285 findings and may reflect adaptive responses to hypoxic-reoxygenation events secondary to
286 reduced utero-placental and/or feto-placental flows in FGR pregnancies (42-44).
287 Morphological findings provide a clue to underlying placental mechanisms that may be subject
288 to change, with the resultant amelioration of disease and improvement to fetal outcome, if they
289 can be enacted *in utero*. There is already significant interest in delivery of targeted agents to
290 the uterine arteries to improve blood flow (45). Delivery of agents to target specific areas of
291 pathology and functional deficit within the placenta to improve the clinical condition may also
292 be a potential therapeutic option.
293
294 Our approach to combine morphological assessments with gene expression aimed to identify
295 some key aetiological pathways for the pathology seen. Expression of placental *IGF2*, *SLC2A3*
296 and *SLC38A1* was lower across the FGR placenta, correlating with volumes and other specific
297 placental features, suggesting a global role for these molecules in placental structure and
298 development in the presence of FGR. Indeed, *IGF2* is known to be important for the formation
299 of the placental exchange interface in humans, among other species (37, 38, 46), and is
300 expressed at lower levels in placentas showing FGR/small for gestational age in some (47, 48),
301 but not all studies (49). Prior work has shown that a genetic deficiency of *SLC2A3* in mice

leads to FGR in mice (36), which supports our findings, but is in contrast to other work reporting an upregulation of its encoded protein in the human placenta of late-onset FGR (50). Of the system A amino acid transporters expressed by the human placenta, *SLC38A1* is key for system A activity at term (51). Other work has also shown that placental system A activity is reduced in explants prepared from term FGR placentas (52). *VEGFA* was significantly lower in the peripheral region of the placenta in FGR and correlated to the following placental pathology (terminal villi, trophoblast and capillary volume) that might suggest a causal association. This is consistent with other work reporting lower placental *VEGFA* expression at term in late onset FGR (53, 54), and the involvement of angiogenic factors more generally in normal and pathological pregnancies (55). Our findings also have relevance for emerging pre-clinical research in placenta-directed gene therapy for FGR, including the utility of insulin-like growth factors and angiogenic regulators (56). *HNF1A* was more highly expressed by the peripheral region compared with central region in healthy, but not FGR placentas. Little is known about the function of *HNF1A* in the placenta, although the human tissue atlas indicates it is abundantly expressed by the villous syncytiotrophoblast (https://www.proteinatlas.org/ENSG00000135100-HNF1A/tissue/placenta). Recent work has highlighted that *HNF1A* may regulate a large number of genes in trophoblast cells (57) and mediate metabolic changes (58), which could be important for the placental support of fetal growth, more broadly.

Using predictive modelling, we demonstrated the potential of predicting outcome (control or FGR) based on stereology and qPCR data, hence, proving a link between the data analysed and functional roles in the placenta. Stereology and qPCR measurements taken from the peripheral part of the placenta, and analysed together, have the highest predictive power. To avoid any possible overfitting of the models, we did not perform any feature selection in advance for

tuning of the algorithm hyperparameters. Despite this, we were able to obtain predictions with very high accuracy, as, in fact, for the best model only one sample out of 60 (4 samples from peripheral placenta part for each of 15 patients) considered was predicted incorrectly. This one sample belonged to a subject (Patient FGR 6) who needed a caesarean section due to an immediate life-threatening situation (Cat1 CS) and was noted to be obese (BMI >35kg/m^2; obese category 2). Indeed, this subject was one that was most likely to be misclassified in all the tested models. Nevertheless, we found that the morphological data clearly shows separation of features for control and FGR placentas and probably, this made it possible to obtain high quality constructed models. For the present study, we used a very strict LOOCV. It did not provide us with one final model but brings the hope that testing our predictive model in a larger dataset, with extremes of pathology, may help improve accuracy and sensitivity of the model developed. Whilst modelling predictions were poor for qPCR data used alone, it is important to mention that adding these data to the analysis of stereology data improved prediction, hence, confirming importance of qPCR data and underlying link of these data with functional features.

Overall, our data add to current understanding of placental function through comprehensive sampling of healthy placentas and those affected by disease (FGR) with careful deep histological analysis, integrated with expression of genes with key biological pathways implicated in poor placental function. Whilst, our modelling approach still requires some validation, with further pathology analysed, it offers the promise of better diagnostic yield and novel insight into biological pathways that affect FGR pregnancies.

Material and methods:

Placental tissue collection and sampling

Subjects were recruited from University College London Hospital NHS Foundation Trust, London, UK with ethics approval from the South-Central Oxford A research ethics committee (17/SC/0432). After written informed consent was obtained, term placental biopsies were collected from subjects diagnosed with late-onset FGR (n=7, FGR detected after 32 weeks' gestation and an estimated fetal weight and/or abdominal circumference below 3rd centile on population-based charts used clinically (59)), and from control subjects with appropriately grown fetuses (n=9 birthweight >10th centile and <90th centile). Data on maternal pre-existing conditions, previous obstetric history, ultrasound examination, and pregnancy complications were collected at the time of recruitment.

Placentas were weighed and sampled within 30 minutes of delivery. Sampling sites were chosen to be representative of four central and four peripheral regions always relative to cord insertion (Figure 4A). In marginal cord insertions, the placenta was orientated with the cord anterior. Sampling then took place relative to the cord insertion as in other cases. This meant there was one site that had less tissue to sample from initially, in non-central cord insertions, but that ultimately the same amount of tissue was sampled, and that tissue selection was directly related to the cord in the same way as all other samples. For each placenta, 8 tissue biopsies (with maternal tissue and fetal chorionic plate removed) were snap frozen using liquid nitrogen or dry ice and stored at -80°C. Neighboring sampling sites were then immersion-fixed in 4% paraformaldehyde.

372 ***RNA extraction, cDNA synthesis and qPCR***

373 Total RNA was extracted from n=9 control and n=6 FGR frozen placental tissues (n=1 FGR
374 sample was not taken due to delay in freezing this sample) using the RNeasy Fibrous Tissue
375 Mini Kit (Qiagen, Hilden, Germany) following the manufacturer's protocol. Briefly,
376 approximately 2mg of tissue was added to 300µl of lysis buffer and homogenized using a bead-
377 based technique. Following treatment with proteinase K and addition of 100% ethanol, the
378 homogenate was transferred to the spin columns, washed with supplied buffers and centrifuged
379 to remove contaminants. Purified RNA was then eluted into RNase-free water. Quality and
380 concentration of extracted RNA were determined by Nanodop (Thermo Fisher Scientific,
381 Waltham, CA, USA).
382
383 Complementary DNA (cDNA) was synthesized using the Applied Biosystems High-Capacity
384 cDNA Reverse Transcription Kit (Thermo Fisher Scientific) according to manufacturer's
385 instructions on a thermal cycler. Real-time PCR was performed in duplicate using TaqMan™
386 Universal Master Mix II, with UNG (Thermo Fisher Scientific) and inventoried TaqMan®
387 gene expression assay probes with either VIC and FAM fluorophores for 5 housekeeping genes
388 (*18SrRNA*, *B2M*, *GAPDH*, *GUSB* and *YWHAZ*) and 8 genes of interest (*HNF1A*, *IGF2*,
389 *SLC2A1*, *SLC2A3*, *SLC38A1*, *SLC38A2*, *SLC38A4* and *VEGFA*) (Table 4). Only stable
390 housekeeping genes (*18S rRNA*, *B2M*, *GADPH* and *YWHAZ*) that showed no statistically
391 significant differences between cases and controls were included in the housekeeper geomean
392 calculation for normalising gene expression across samples. The relative expression of genes
393 of interest was then calculated using the $2^{-\Delta\Delta Ct}$ method.
394

395 ***Histological preparation***

396 Following paraformaldehyde fixation, biopsies of 8 sites from each control (n=9) and FGR
397 (n=7) placenta were embedded in paraffin using routine histological techniques and sectioned
398 at 7µm thickness. Sections were rehydrated using xylene and ethanol gradients, stained with
399 haematoxylin and eosin, dehydrated with ethanol gradients and xylene, then mounted with
400 DPX. Slides were then scanned using a Nanozoomer digital slide scanner (Hamamatsu
401 Photonics, Shizuoka Prefecture, Japan).

402

403 ***Placental stereology***

404 Placentas were analysed blinded to the diagnosis of FGR. To perform stereological analysis in
405 a manner similar to that performed previously (60); transparent lattices with test points, test
406 lines or test arcs were superimposed onto scanned images viewed under different magnification
407 on the NDP.view2 software (Hamamatsu Photonics). Volume densities of the intervillous
408 space, stem villi, intermediate villi, terminal villi, syncytial knots, and fibrosis (Figure 4B-C)
409 were estimated by point counting and a lattice of equally spaced test points arranged 4 by 4
410 under 10X magnification in at least 13 fields of view for a minimum of 200 measurements per
411 section. Volume densities of the trophoblast, stroma, and fetal capillaries (Figure 4D) within
412 villi were estimated under a similar lattice under 40X magnification in 20 fields of view per
413 sample. Absolute placental volumes were estimated by multiplying volume densities with
414 placental weight (g). Arithmetic barrier thickness was assessed under 100X magnification in
415 20 fields of view per sample and a superimposed lattice with equally spaced straight test lines,
416 which at times, intersected fetal capillary and villous trophoblast involved in exchange. The
417 'measure' tool within the software was then used to determine the shortest distance between a
418 fetal capillary and the maternal blood space, where there was an intersection. Mean harmonic
419 barrier thickness was calculated using the inverse of mean reciprocal of each raw arithmetic

barrier thickness measurement. Thickness uniformity index, as a measure of the variability in thickness across the villous membrane, was obtained from the ratio of the mean arithmetic barrier thickness to the mean harmonic barrier thickness. Surface densities were approximated by counting chance intersections of fetal capillaries and villous trophoblast involved in exchange with superimposed test arc lines under 40X magnification. To derive surface areas, surface densities were multiplied by placental villous volume. The theoretical diffusion capacity was calculated using the total surface area for exchange (averaged surface area of fetal capillaries and villi) divided by the mean harmonic barrier thickness and multiplied by Krogh's constant for oxygen diffusion. Specific diffusion capacity was then calculated by dividing the theoretical diffusion capacity by the infant birthweight.

Predictive modelling

To evaluate the informativity of different placental sampling locations (only peripheral, only central or both regions together) and different data types (only stereological data, only PCR data or both types together), we studied all their possible combinations with analysis performed in R (version 4.0.2). To analyse several well-established multi-dimensional methods of data analysis, the machine learning models (*xgbTree*, *glmnet* and *nnet*) were implemented using *caret* package (version 6.0.90). All 27 models were trained with default set of hyperparameters, cross-validated on 5 folds (for a better selection of internal algorithm parameters), with seed parameter set to 123. The performance of models was assessed with receiver operating characteristic (ROC) curves using area under the curve (AUC) with 95% confidence intervals (*pROC* package, version 1.18.0). Results of AUCs were presented in two ways:

- *All sample's AUC* - Calculating AUC considering all samples as independent;

- *All patient's AUC* - Calculating AUC on patient's result's only (if all samples belonging to one patient were correctly predicted, then we assumed that a prediction for this patient was correct, if the prediction was wrong in at least one sample of the sample's patient, then it was set as wrong for this patient).

For illustration of interdependencies of features, which are presented in Supplementary Figure 1, we selected the best pairs that showed significant differences between FGR and control groups using ANOVA test after applying FDR (false discovery rate) adjustment to test's p-values (*stats* package, Version 4.0.2).

Statistical analyses

Normality of data was assessed by D'Agostino-Pearson normality test. ROUT testing for outliers was used to identify any outliers, which were then excluded from the analysis. For comparisons between 2 groups, Student's t tests and Mann-Whitney U tests were performed for parametric and non-parametric continuous data, respectively. Categorical data between FGR and controls were analysed by a 2 X 2 contingency table with Fisher's Exact Test. Two-way ANOVAs followed by Sidak post hoc test for multiple comparisons were used to analyse mRNA expression data by pathology and sampling location. Graphpad Prism 6.01 (Graphpad Software Inc., La Jolla, CA, USA) was used for statistical analyses. A p-value of <0.05 was considered statistically significant for clinical characteristics and mRNA expression analysis. To account for multiple testing in histological analyses, a false discovery rate correction at 5% was applied to determine statistical significance.

Study approval

Subjects were recruited from University College London Hospital NHS Foundation Trust, London, UK with ethics approval from the South-Central Oxford A research ethics committee

(17/SC/0432) and the Stanmore research ethics committee (13/LO/1254). Written informed consent was received prior to participation.

Author contributions

HEJY, KM, SLH and ANSP designed the study. HEJY, KM, MABY, ESP collected and/or performed experiments. HEJY, KM, ESP and TN analysed and graphed the data. TN and AZ provided predictive modelling analysis. HEJY, KM, TN, AZ, ALD, SLH and ANSP interpreted the data. HEJY, KM, SLH and ANSP wrote the paper. All authors performed final editing checks and approved the final manuscript.

Acknowledgements

ANSP received funding for this work via an Academy of Medical Sciences Springboard Grant, Royal Society Dorothy Hodgkin Research Fellowship (DH130036/RG74249), MRC New Investigator Grant (MR/R022690/1/RG93186) and Lister Institute of Preventative Medicine Research Prize (RG93692). TN and AZ are supported by a Medical Research Council grant (MR/R02524X/1). HEJY was supported by an A*STAR International Fellowship from the Agency for Science, Technology and Research. KM was supported by UCLH Charity. SLH received funding for this work via an Academy of Medical Sciences Clinical Lecturer Starter Grant (AMS-SGL015\ 1011) and the UCLH EGA Obstetric Charity.

Data availability

All data produced in the present study are available upon reasonable request to the authors.

References

1. Napso T, Yong HE, Lopez-Tello J, and Sferruzzi-Perri AN. The role of placental hormones in mediating maternal adaptations to support pregnancy and lactation. *Front Physiology.* 2018;9:1091.

2. Burton GJ, Fowden AL, and Thornburg KL. Placental Origins of Chronic Disease. *Physiol Rev.* 2016;96(4):1509-65.

3. Byrne M, Aughwane R, James JL, Hutchinson JC, Arthurs OJ, Sebire NJ, et al. Structure-function relationships in the feto-placental circulation from in silico interpretation of micro-CT vascular structures. *J Theor Biol.* 2021;517:110630.

4. Aughwane R, Schaaf C, Hutchinson JC, Virasami A, Zuluaga MA, Sebire N, et al. Micro-CT and histological investigation of the spatial pattern of feto-placental vascular density. *Placenta.* 2019;88:36-43.

5. Lawn JE, Blencowe H, Oza S, You D, Lee AC, Waiswa P, et al. Every Newborn: progress, priorities, and potential beyond survival. *Lancet.* 2014;384(9938):189-205.

6. Sharma D, Shastri S, and Sharma P. Intrauterine Growth Restriction: Antenatal and Postnatal Aspects. *Clinical medicine insights Pediatrics.* 2016;10:67-83.

7. Gordijn SJ, Beune IM, Thilaganathan B, Papageorghiou A, Baschat AA, Baker PN, et al. Consensus definition of fetal growth restriction: a Delphi procedure. *Ultrasound Obstet Gynecol.* 2016;48(3):333-9.

8. Van den Berg BJ, and Yerushalmy J. The relationship of the rate of intrauterine growth of infants of low birth weight to mortality, morbidity, and congenital anomalies. *J Pediatr.* 1966;69(4):531-45.

9. Bianchi ME, and Restrepo JM. Low Birthweight as a Risk Factor for Non-communicable Diseases in Adults. *Front Med (Lausanne).* 2021;8:793990.

10. Caradeux J, Martinez-Portilla RJ, Basuki TR, Kiserud T, and Figueras F. Risk of fetal death in growth-restricted fetuses with umbilical and/or ductus venosus absent or reversed end-diastolic velocities before 34 weeks of gestation: a systematic review and meta-analysis. *Am J Obstet Gynecol.* 2018;218(2S):S774-S82 e21.

11. Ishihara N, Matsuo H, Murakoshi H, Laoag-Fernandez JB, Samoto T, and Maruo T. Increased apoptosis in the syncytiotrophoblast in human term placentas complicated by either preeclampsia or intrauterine growth retardation. *Am J Obstet Gynecol.* 2002;186(1):158-66.

12. Mayhew TM, Wijesekara J, Baker PN, and Ong SS. Morphometric evidence that villous development and fetoplacental angiogenesis are compromised by intrauterine growth restriction but not by pre-eclampsia. *Placenta.* 2004;25(10):829-33.

13. Macara L, Kingdom JC, Kaufmann P, Kohnen G, Hair J, More IA, et al. Structural analysis of placental terminal villi from growth-restricted pregnancies with abnormal umbilical artery Doppler waveforms. *Placenta.* 1996;17(1):37-48.

14. Teasdale F, and Jean-Jacques G. Intrauterine growth retardation: morphometry of the microvillous membrane of the human placenta. *Placenta.* 1988;9(1):47-55.

15. Burton GJ, and Fowden AL. The placenta: a multifaceted, transient organ. *Philosophical transactions of the Royal Society of London Series B, Biological sciences.* 2015;370(1663):20140066.

16. Chavatte-Palmer P, and Tarrade A. Placentation in different mammalian species. *Ann Endocrinol (Paris).* 2016;77(2):67-74.

17. Pere MC. Materno-foetal exchanges and utilisation of nutrients by the foetus: comparison between species. *Reprod Nutr Dev.* 2003;43(1):1-15.

18. Crawford MA, Hassam AG, and Williams G. Essential fatty acids and fetal brain growth. *Lancet.* 1976;1(7957):452-3.

19. Gresham EL, Simons PS, and Battaglia FC. Maternal-fetal urea concentration difference in man: metabolic significance. *J Pediatr.* 1971;79(5):809-11.

20. Sferruzzi-Perri AN, Vaughan OR, Coan PM, Suciu MC, Darbyshire R, Constancia M, et al. Placental-specific Igf2 deficiency alters developmental adaptations to undernutrition in mice. *Endocrinology.* 2011;152(8):3202-12.

21. Sferruzzi-Perri AN, Vaughan OR, Haro M, Cooper WN, Musial B, Charalambous M, et al. An obesogenic diet during mouse pregnancy modifies maternal nutrient partitioning and the fetal growth trajectory. *FASEB.* 2013;27(10):3928-37.

22. Vaughan OR, Sferruzzi-Perri AN, and Fowden AL. Maternal corticosterone regulates nutrient allocation to fetal growth in mice. *Journal of Physiology.* 2012;590(21):5529-40.

23. Higgins JS, Vaughan OR, de Liger EF, Fowden AL, and Sferruzzi-Perri AN. Placental phenotype and resource allocation to fetal growth are modified by the timing and degree of hypoxia during mouse pregnancy. *J Physiol.* 2015;594(5):1341-56.

24. Napso T, Hung YP, Davidge ST, Care AS, and Sferruzzi-Perri AN. Advanced maternal age compromises fetal growth and induces sex-specific changes in placental phenotype in rats. *Sci Rep.* 2019;9(1):16916.

25. Lewis RM, and Sferruzzi-Perri AN. In: Poston L, Godfrey KM, Hanson MA, and Gluckman P eds. *Developmental Origins of Health and Disease*. Cambridge University Press.

26. Audette MC, McLaughlin K, and Kingdom JC. Second Trimester Placental Growth Factor Levels and Placental Histopathology in Low-Risk Nulliparous Pregnancies. *J Obstet Gynaecol Can.* 2021;43(10):1145-52 e1.

27. Burton GJ, Sebire NJ, Myatt L, Tannetta D, Wang YL, Sadovsky Y, et al. Optimising sample collection for placental research. *Placenta.* 2014;35(1):9-22.

28. Mayhew TM. Taking tissue samples from the placenta: an illustration of principles and strategies. *Placenta.* 2008;29(1):1-14.

29. Mayhew TM. Morphomics: An integral part of systems biology of the human placenta. *Placenta.* 2015;36(4):329-40.

30. Salafia CM, Yampolsky M, Misra DP, Shlakhter O, Haas D, Eucker B, et al. Placental surface shape, function, and effects of maternal and fetal vascular pathology. *Placenta.* 2010;31(11):958-62.

31. Gordon Z, Elad D, Almog R, Hazan Y, Jaffa AJ, and Eytan O. Anthropometry of fetal vasculature in the chorionic plate. *J Anat.* 2007;211(6):698-706.

32. Heifetz SA. The umbilical cord: obstetrically important lesions. *Clin Obstet Gynecol.* 1996;39(3):571-87.

33. Sferruzzi-Perri AN, and Camm EJ. The programming power of the placenta. *Frontiers in Physiology.* 2016;7:33.

34. Vaughan OR, Maksym K, Silva E, Barentsen K, Anthony RV, Brown TL, et al. Placenta-specific Slc38a2/SNAT2 knockdown causes fetal growth restriction in mice. *Clin Sci (Lond).* 2021;135(17):2049-66.

35. Luscher BP, Marini C, Joerger-Messerli MS, Huang X, Hediger MA, Albrecht C, et al. Placental glucose transporter (GLUT)-1 is down-regulated in preeclampsia. *Placenta.* 2017;55:94-9.

36. Ganguly A, McKnight RA, Raychaudhuri S, Shin BC, Ma Z, Moley K, et al. Glucose transporter isoform-3 mutations cause early pregnancy loss and fetal growth restriction. *Am J Physiol Endocrinol Metab.* 2007;292(5):E1241-55.

589 37. Sferruzzi-Perri AN, Owens JA, Pringle KG, and Roberts CT. The neglected role of
590 insulin-like growth factors in the maternal circulation regulating fetal growth. *Journal*
591 *of Physiology* 2010;589(Pt 1):7-20.
592 38. Sferruzzi-Perri AN, Sandovici I, Constancia M, and Fowden AL. Placental phenotype
593 and the insulin-like growth factors: resource allocation to fetal growth. *Journal of*
594 *Physiology.* 2017;595(15):5057-93.
595 39. Mifsud W, and Sebire NJ. Placental pathology in early-onset and late-onset fetal
596 growth restriction. *Fetal Diagn Ther.* 2014;36(2):117-28.
597 40. Brosens I, Pijnenborg R, Vercruysse L, and Romero R. The "Great Obstetrical
598 Syndromes" are associated with disorders of deep placentation. *Am J Obstet Gynecol.*
599 2011;204(3):193-201.
600 41. Burton GJ, and Jauniaux E. Pathophysiology of placental-derived fetal growth
601 restriction. *Am J Obstet Gynecol.* 2018;218(2S):S745-S61.
602 42. Kovo M, Schreiber L, Ben-Haroush A, Wand S, Golan A, and Bar J. Placental
603 vascular lesion differences in pregnancy-induced hypertension and normotensive fetal
604 growth restriction. *Am J Obstet Gynecol.* 2010;202(6):561 e1-5.
605 43. Colson A, Sonveaux P, Debieve F, and Sferruzzi-Perri AN. Adaptations of the human
606 placenta to hypoxia: opportunities for interventions in fetal growth restriction. *Hum*
607 *Reprod Update.* 2020.
608 44. Cindrova-Davies T, and Sferruzzi-Perri AN. Human placental development and
609 function. *Seminars in Cell and Developmental Biology.* 2022;In press.
610 45. David AL, Torondel B, Zachary I, Wigley V, Abi-Nader K, Mehta V, et al. Local
611 delivery of VEGF adenovirus to the uterine artery increases vasorelaxation and
612 uterine blood flow in the pregnant sheep. *Gene Ther.* 2008;15(19):1344-50.

46. Sferruzzi-Perri AN. Regulating needs: Exploring the role of insulin-like growth factor-2 signalling in materno-fetal resource allocation. *Placenta.* 2018;Suppl 1:S16-S22.

47. Guo L, Choufani S, Ferreira J, Smith A, Chitayat D, Shuman C, et al. Altered gene expression and methylation of the human chromosome 11 imprinted region in small for gestational age (SGA) placentae. *Dev Biol.* 2008;320(1):79-91.

48. Yamaguchi Y, Tayama C, Tomikawa J, Akaishi R, Kamura H, Matsuoka K, et al. Placenta-specific epimutation at H19-DMR among common pregnancy complications: its frequency and effect on the expression patterns of H19 and IGF2. *Clin Epigenetics.* 2019;11(1):113.

49. Antonazzo P, Alvino G, Cozzi V, Grati FR, Tabano S, Sirchia S, et al. Placental IGF2 Expression in Normal and Intrauterine Growth Restricted (IUGR) Pregnancies. *Placenta.* 2008;29(1):99-101.

50. Janzen C, Lei MY, Cho J, Sullivan P, Shin BC, and Devaskar SU. Placental glucose transporter 3 (GLUT3) is up-regulated in human pregnancies complicated by late-onset intrauterine growth restriction. *Placenta.* 2013;34(11):1072-8.

51. Desforges M, Greenwood SL, Glazier JD, Westwood M, and Sibley CP. The contribution of SNAT1 to system A amino acid transporter activity in human placental trophoblast. *Biochem Biophys Res Commun.* 2010;398(1):130-4.

52. Shibata E, Hubel CA, Powers RW, von Versen-Hoeynck F, Gammill H, Rajakumar A, et al. Placental System A Amino Acid Transport is Reduced in Pregnancies With Small For Gestational Age (SGA) Infants but Not in Preeclampsia with SGA Infants. *Placenta.* 2008;29(10):879-82.

636 53. Lash G, MacPherson A, Liu D, Smith D, Charnock-Jones S, and Baker P. Abnormal
637 fetal growth is not associated with altered chorionic villous expression of vascular
638 endothelial growth factor mRNA. *Mol Hum Reprod.* 2001;7(11):1093-8.
639 54. Lyall F, Young A, Boswell F, Kingdom JC, and Greer IA. Placental expression of
640 vascular endothelial growth factor in placentae from pregnancies complicated by pre-
641 eclampsia and intrauterine growth restriction does not support placental hypoxia at
642 delivery. *Placenta.* 1997;18(4):269-76.
643 55. Andraweera PH, Dekker GA, and Roberts CT. The vascular endothelial growth factor
644 family in adverse pregnancy outcomes. *Hum Reprod Update.* 2012;18(4):436-57.
645 56. Krishnan T, and David AL. Placenta-directed gene therapy for fetal growth
646 restriction. *Semin Fetal Neonatal Med.* 2017;22(6):415-22.
647 57. Ducat A, Vargas A, Doridot L, Bagattin A, Lerner J, Vilotte JL, et al. Low-dose
648 aspirin protective effects are correlated with deregulation of HNF factor expression in
649 the preeclamptic placentas from mice and humans. *Cell Death Discov.* 2019;5:94.
650 58. Rout M, and Lulu SS. Molecular and disease association of gestational diabetes
651 mellitus affected mother and placental datasets reveal a strong link between insulin
652 growth factor (IGF) genes in amino acid transport pathway: A network biology
653 approach. *J Cell Biochem.* 2018.
654 59. Brenner WE, Edelman DA, and Hendricks CH. A standard of fetal growth for the
655 United States of America. *Am J Obstet Gynecol.* 1976;126(5):555-64.
656 60. Mayhew TM. Stereology and the placenta: where's the point? -- a review. *Placenta.*
657 2006;27 Suppl A:S17-25.

658

659

660 **Table 1: Patient characteristics.**

Characteristics	Control (N=9)	FGR (N=7)	P-value
Maternal age	34.44 ± 1.84	32.00 ± 1.16	0.339
Maternal ethnicity	8 white, 1 non-white	2 white, 5 non-white	0.035
Booking BMI (kg/m^2)	24.67 ± 1.51	24.47 ± 2.75	0.946
Mode of delivery	4 vaginal deliveries, 5 caesarean sections	2 vaginal deliveries, 5 caesarean sections,	0.620
Gestational age at delivery (weeks)	39.14 (39.07 – 39.79)	38.29 (37.29 – 39.00)	0.006
Infant sex	4F, 5M	2F, 5M	0.633
Infant birthweight (kg)	3.53 ± 0.13	2.33 ± 0.18	< 0.001
Placental weight (g)	478.9 ± 16.6	340.7 ± 31.0	0.001

661 Data are presented as mean ± SEM and were analysed by Student's t test or Mann-Whitney U
662 test. Categorical data were analysed by 2 X 2 contingency table with Fisher's Exact Test. BMI,
663 body mass index; F, female; M, male.
664

665 **Table 2: Morphological differences in the placenta by pathology**

	Control (N=9)	**FGR (N=7)**	**P-value (^FDR)**
Volume density (cm^3/g)			
Intervillous space	0.37±0.01	0.36±0.02	0.447
Stem villi	0.06±0.01	0.06±0.01	0.895
Intermediate villi	0.12±0.01	0.08±0.01	0.008*
Terminal villi	0.42±0.02	0.4±0.03	0.474
Syncytial knots	0.02±0.00	0.01±0.00	0.002*
Fibrosis	0.01±0.01	0.1±0.02	0.001*
Trophoblast	0.32±0.01	0.34±0.03	0.583
Stromal	0.55±0.02	0.45±0.05	0.058
Capillary	0.13±0.01	0.21±0.03	0.016*
Volume (cm^3)			
Intervillous space	179.73±9.45	119.44±10.77	0.001*
Stem villi	27.83±3.2	20.17±4.25	0.163
Intermediate villi	55.4±4.41	25.48±2.43	<0.001*
Terminal villi	200.73±10.54	135.3±16.23	0.003*
Syncytial knots	8.39±0.78	2.44±0.71	<0.001*
Fibrosis	5.88±3.24	37.02±7.43	0.001*
Trophoblast	153.5±6.83	114.7±13.69	0.017*
Stromal	263.09±15.46	153.23±21.66	0.001*
Capillary	62.3±5.04	72.78±13.76	0.445
Barrier thickness (µm)			

Arithmetic mean	2.83±0.08	2.85±0.18	0.912
Harmonic mean	2.14±0.07	2.24±0.14	0.500
Thickness uniformity index (a measure of thickness variability)	1.32±0.01	1.48±0.08	0.044
Surface density (cm^2/cm^3)			
Villi	610.45±23.85	630.28±44.68	0.683
Fetal capillary	298.26±19.81	401.92±48.29	0.048
Surface area (m^2)			
Villi	11.68±2.88	10.59±1.55	0.009*
Fetal capillary	6.27±1.7	6.89±1.23	0.576
Theoretical diffusion capacity (cm^2/min/kPa)	95.29±4.86	70.26±11.5	0.047
Specific diffusion capacity (cm^2/min/kPa/g)	27.2±1.49	29.47±3.99	0.567

Data presented as mean ± SEM and analysed by t test with FDR (false discovery correction) correction at 5%. * Denotes significant findings that passed the 5% FDR.

669 **Table 3: Predictive modelling results using different machine learning methods.**

Peripheral & Central									
	Stereology			qPCR			Stereology & qPCR		
	xgbTree	glmnet	nnet	xgbTree	glmnet	nnet	xgbTree	glmnet	nnet
AUC for all samples	0.899	0.913	0.927	0.705	0.733	0.719	0.875	0.92	0.948
AUC for all patients	0.611	0.861	0.917	0.639	0.528	0.528	0.694	0.861	0.917
Peripheral									
	Stereology			qPCR			Stereology & qPCR		
	xgbTree	glmnet	nnet	xgbTree	glmnet	nnet	xgbTree	glmnet	nnet
AUC for all samples	0.903	0.938	0.924	0.681	0.694	0.681	0.819	0.938	**0.979**
AUC for all patients	0.861	0.917	0.861	0.556	0.556	0.556	0.778	0.917	**0.917**
Central									
	Stereology			qPCR			Stereology & qPCR		
	xgbTree	glmnet	nnet	xgbTree	glmnet	nnet	xgbTree	glmnet	nnet
AUC for all samples	0.889	0.903	0.903	0.722	0.694	0.722	0.826	0.889	0.889

AUC for all patients	0.778	0.861	0.861	0.611	0.611	0.611	0.722	0.861	0.806

Results for each combination of "placenta part + type of measurement + ML model" The best version of the model is *nnet* model (highlighted in bold) on peripheral parts of placenta using stereological and qPCR data together. In this case, "AUC for all patients" = 0.917 (corresponding to an error for just one patient-case in a sample of 15 patients: 9 controls and 6 FGR), and "AUC for all samples" = 0.979 (corresponding to an error for only one measurement, a FGR in a set of 15*4 samples: 9*4 control samples and 6*4 FGR samples). A complete table of errors is given in Supplementary Table 3.

679 **Table 4 Probes used for real-time PCR**

Analysed genes	**Gene symbol**	**Probe ID**	**Fluorophore**
Housekeeping genes	*18S rRNA*	Hs99999901_s1	VIC
	B2M	Hs00187842_m1	VIC
	GAPDH	Hs02786624_g1	VIC
	GUSB	Hs00939627_m1	VIC
	YWHAZ	Hs01122445_g1	VIC
Genes of interest	*HNF1A*	Hs00167041_m1	VIC
	IGF2	Hs04188276_m1	FAM
	SLC2A1	Hs00892681_m1	FAM
	SLC2A3	Hs00359840_m1	FAM
	SLC38A1	Hs01562175_m1	FAM
	SLC38A2	Hs01089954_m1	VIC
	SLC38A4	Hs00394339_m1	FAM
	VEGFA	Hs00900055_m1	FAM

680

681

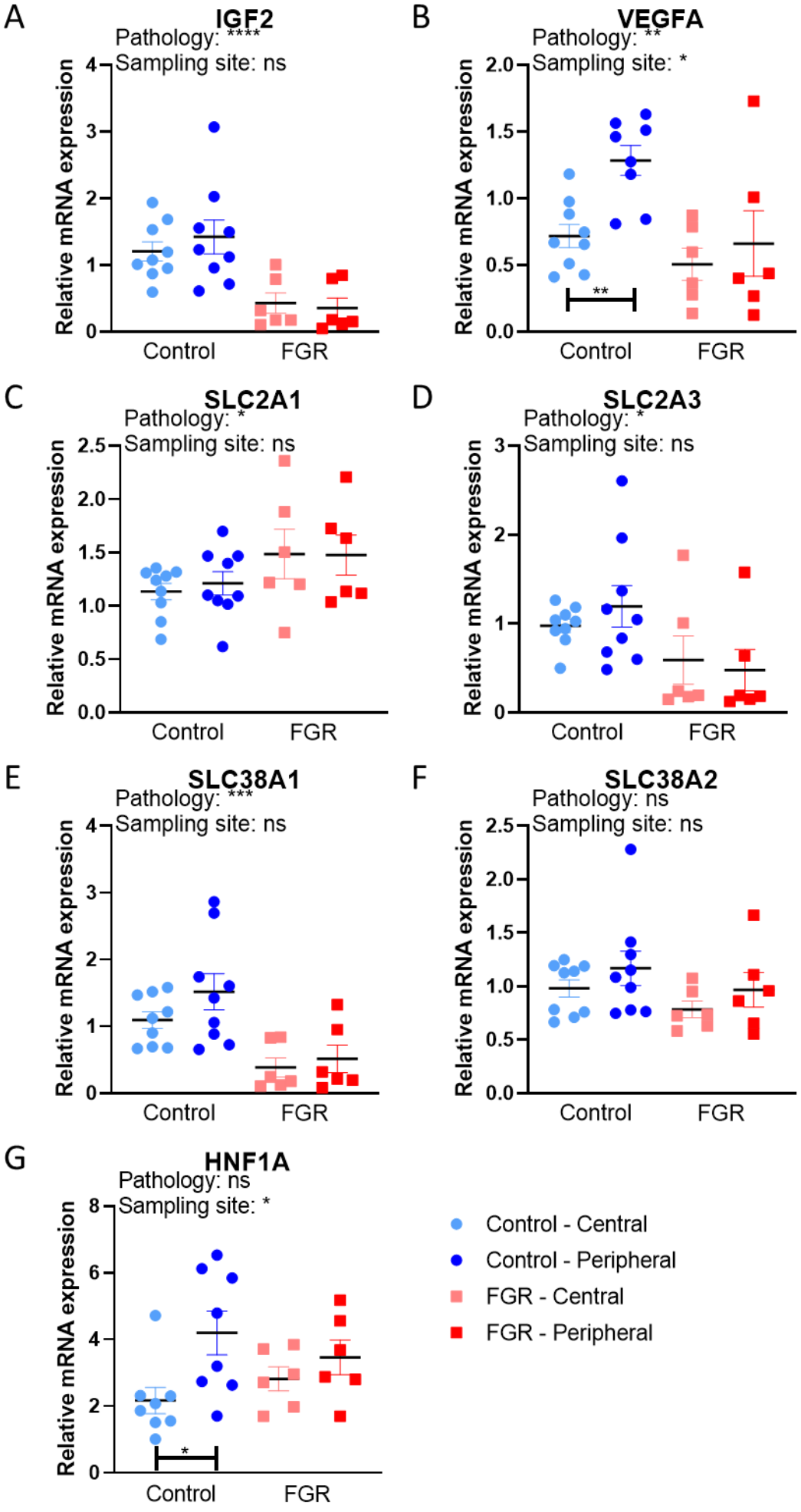

682

683 **Figure 1: Relative mRNA expression of selected growth factors and nutrient transporters**
684 **in control and FGR placentas.** Expression of growth factors (*IGF2*, *VEGFA*), and
685 transporters (*SLC2A1*, *SLC2A3*, *SLC38A1*, *SLC38A2* and the transcription factor *HNF1A*, were
686 evaluated by qPCR. A total of 3 outliers were excluded; 1 control peripheral value for *VEGFA*,
687 and 1 control central value and 1 control peripheral value for *HNF1A*. Data are presented with
688 individual data points with mean ± SEM and analysed with two-way ANOVA, followed by
689 Sidak's post hoc test for multiple comparisons. *p<0.05, **p<0.01, ***p<0.001,
690 ****p<0.0001.
691

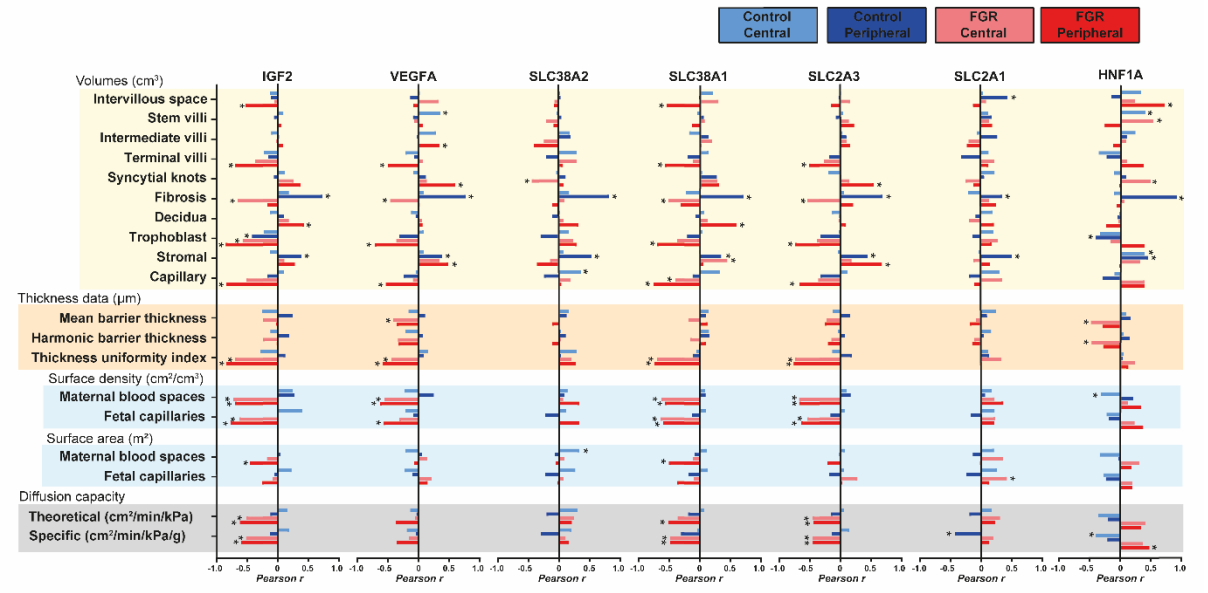

Figure 2. Correlations between stereological parameters and the relative expression of functional genes in the placenta. Pearson's r coefficient was plotted and used to indicate strength of relationship between data (0: low, 1: high) and direction of correlation (+ sign: direct correlation and – sign: inverse correlation). Analysis was performed on each sampling site and experimental group (control and FGR) separately. Sample size was 36 for control and 24 for FGR. *: $p < 0.05$, correlation is statistically significant.

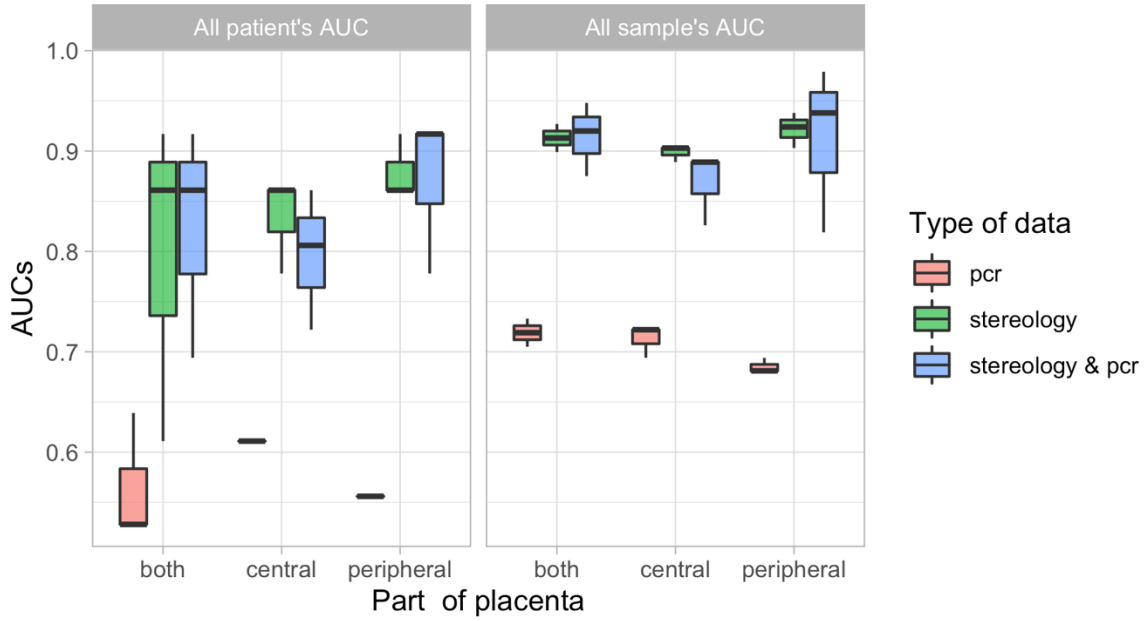

700

701 **Figure 3: Distributions of AUCs, i.e., the performance results of different types of models**
702 **on different types of data obtained on different parts of the placenta for all patients and**
703 **for all their measurements separately.**

704

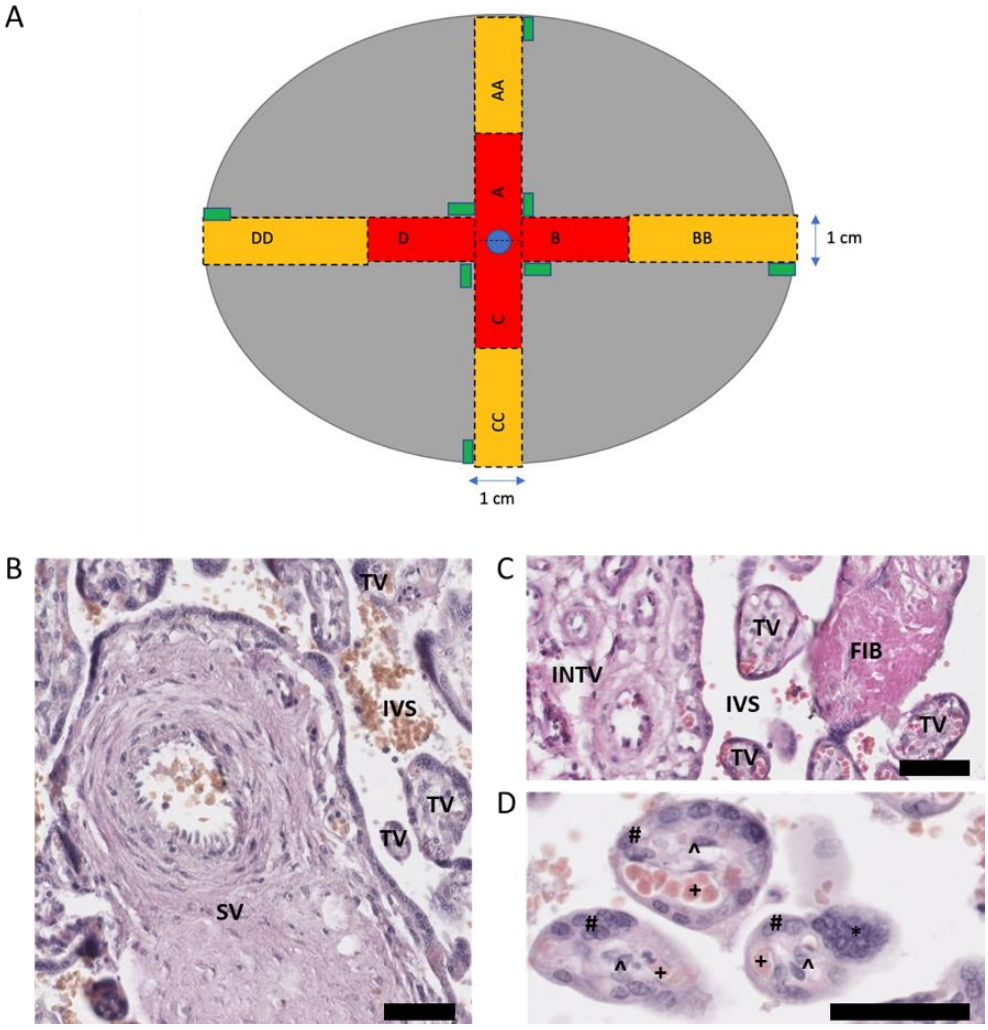

Figure 4. Diagram showing sampling of placenta (A) and main parameters measured in histological sections of placenta (B-D). (**A**) Dotted lines indicate where the placenta should be cut with a sterile histology knife. Red boxes with single letters indicate inner sections. Yellow boxes with double letters indicate outer sections. Green rectangles represent samples taken for RNA sampling. The central blue circle represents the umbilical cord (cut). (**B-D**) Representative histological sections of term human placenta. Stereological analysis was performed by identifying the intervillous space (IVS), stem villi (SV), intermediate villi (INTV), terminal villi (TV), fibrosis (FIB), syncytial knots (*); and under higher magnification of terminal villi, the trophoblast cell layer (#), fetal capillaries (+) and stromal cells (^). The scale bar denotes 50µm.